

Theory and Phenomenology of Instantons at HERA*

A. Ringwald and F. Schrempp

Deutsches Elektronen-Synchrotron DESY, Hamburg, Germany

Abstract

We review our on-going theoretical and phenomenological investigation of the prospects to discover QCD-instantons in deep-inelastic scattering at HERA.

*Contribution to the Ringberg Workshop “New Trends in HERA Physics”, Ringberg Castle, Tegernsee, Germany, May 30 - June 4, 1999; to be published in the Proceedings.

1 Introduction

It is a remarkable fact that non-Abelian gauge fields in four Euclidean space-time dimensions carry an integer topological charge. Instantons [1] (anti-instantons) are classical solutions of the Euclidean Yang-Mills equations and also represent the simplest non-perturbative fluctuations of gauge fields with topological charge $+1$ (-1). In QCD, instantons are widely believed to play an essential rôle at long distance: They provide a solution of the axial $U(1)$ problem [2], and there seems to be some evidence that they induce chiral symmetry breaking and affect the light hadron spectrum [3]. Nevertheless, a direct experimental observation of instanton-induced effects is still lacking up to now.

Deep-inelastic scattering at HERA offers a unique window to discover QCD-instanton induced events directly through their characteristic final-state signature [4, 5, 6, 7] and a sizeable rate, calculable within instanton perturbation theory [8, 9, 10]. It is the purpose of the present contribution to review our theoretical and phenomenological investigation of the prospects to trace QCD-instantons at HERA.

The outline of this review is as follows:

We start in Sect. 2 with a short introduction to instanton physics, concentrating especially on two important building blocks of instanton perturbation theory, namely the instanton size distribution and the instanton-anti-instanton interaction. A recent comparison [11] of the perturbative predictions of these quantities with their non-perturbative measurements on the lattice [12] is emphasized. It allows to extract important information about the range of validity of instanton perturbation theory. The special rôle of deep-inelastic scattering in instanton physics is outlined in Sect. 3: The Bjorken variables of instanton induced hard scattering processes probe the instanton size distribution and the instanton-anti-instanton interaction [8, 9]. By final state cuts in these variables it is therefore possible to stay within the region of applicability of instanton perturbation theory, inferred from our comparison with the lattice above. Moreover, within this fiducial kinematical region, one is able to predict the rate and the (partonic) final state. We discuss the properties of the latter as inferred from our Monte Carlo generator QCDINS [5, 13]. In Sect. 4, we report on a possible search strategy for instanton-induced processes in deep-inelastic scattering at HERA [7].

2 Instantons in the QCD Vacuum

In this section let us start with a short introduction to instantons and their properties, both in the perturbative as well as in the non-perturbative regime. We shall concentrate on those aspects that will be important for the description of instanton-induced scattering processes in deep-inelastic scattering in Sect. 3. In particular, we shall report on our recent determination of the region of applicability of instanton perturbation theory for the instanton size distribution and the instanton-anti-instanton interaction [11]. Furthermore, we elucidate the connection of instantons with the axial anomaly.

Instantons [1], being solutions of the Yang-Mills equations in Euclidean space, are minima of the Euclidean action S . Therefore, they appear naturally as generalized saddle-points in the Euclidean path integral formulation of QCD, according to which the expectation value of an observable \mathcal{O} is given by

$$\langle \mathcal{O}[A, \psi, \bar{\psi}] \rangle = \frac{1}{Z} \int [dA][d\psi][d\bar{\psi}] \mathcal{O}[A, \psi, \bar{\psi}] e^{-S[A, \psi, \bar{\psi}]}, \quad (1)$$

where the normalization,

$$Z = \int [dA][d\psi][d\bar{\psi}] e^{-S[A, \psi, \bar{\psi}]}, \quad (2)$$

denotes the partition function. Physical observables (e.g. S -matrix elements) are obtained from the Euclidean expectation values (1) by analytical continuation to Minkowski space-time. In particular, the partition function (2) corresponds physically to the vacuum-to-vacuum amplitude.

Instanton perturbation theory results from the generalized saddle-point expansion of the path integral (1) about non-trivial minima of the Euclidean action¹. It can be shown that these non-trivial solutions have integer topological charge,

$$Q \equiv \frac{\alpha_s}{2\pi} \int d^4x \frac{1}{2} \text{tr}(F_{\mu\nu} \tilde{F}_{\mu\nu}) = \pm 1, \pm 2, \dots, \quad (3)$$

and that their action is a multiple of $2\pi/\alpha_s$,

$$S \equiv \int d^4x \frac{1}{2} \text{tr}(F_{\mu\nu} F_{\mu\nu}) = \frac{2\pi}{\alpha_s} |Q| = \frac{2\pi}{\alpha_s} \cdot (1, 2, \dots). \quad (4)$$

In the weak coupling regime, $\alpha_s \ll 1$, the dominant saddle-point has $|Q| = 1$. The solution corresponding to $Q = 1$ is given by² [1] (singular gauge)

$$A_\mu^{(I)}(x; \rho, U, x_0) = -\frac{i}{g} \frac{\rho^2}{(x - x_0)^2} U \frac{\sigma_\mu (\bar{x} - \bar{x}_0) - (x_\mu - x_{0\mu})}{(x - x_0)^2 + \rho^2} U^\dagger, \quad (5)$$

where the ‘‘collective coordinates’’ ρ , x_0 and U denote the size, position and colour orientation of the solution. The solution (5) has been called ‘‘instanton’’ (I), since it is localized in Euclidean space and time (‘‘instantaneous’’), as can be seen from its Lagrange density,

$$\mathcal{L} \left(A_\mu^{(I)}(x; \rho, U, x_0) \right) = \frac{12}{\pi\alpha_s} \cdot \frac{\rho^4}{((x - x_0)^2 + \rho^2)^4} \Rightarrow S \left[A_\mu^{(I)} \right] = \frac{2\pi}{\alpha_s}. \quad (6)$$

It appears as a spherical symmetric bump of size ρ centred at x_0 .

The natural starting point of instanton perturbation theory is the evaluation of the instanton contribution to the partition function (2) [2], by expanding the path integral about the instanton (5).

¹Perturbative QCD is obtained from an expansion about the perturbative vacuum solution, i.e. vanishing gluon field and vanishing quark fields and thus vanishing Euclidean action.

²In Eq. (5) and throughout the paper we use the abbreviations, $v \equiv v_\mu \sigma^\mu$, $\bar{v} \equiv v_\mu \bar{\sigma}^\mu$ for any four-vector v_μ .

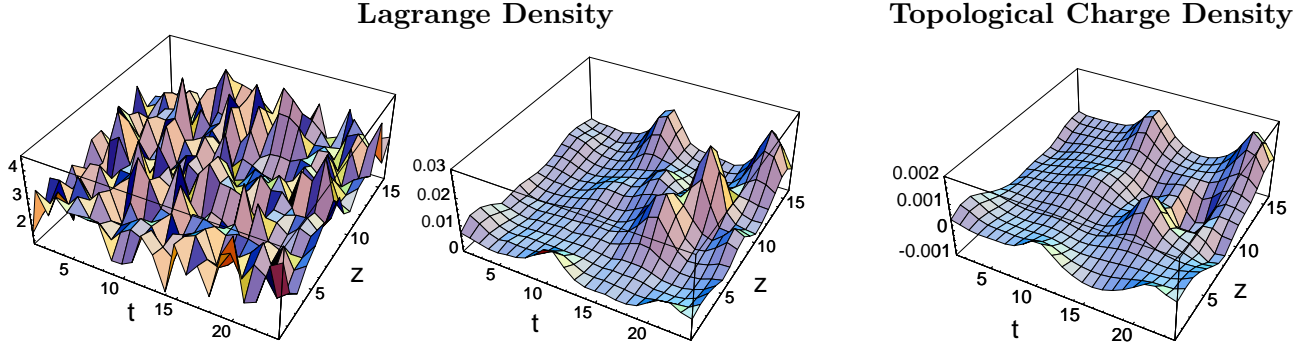


Figure 1: Instanton content of a typical slice of a gluon configuration on the lattice at fixed x , y as a function of z and t [17]. Lagrange density before “cooling”, with fluctuations of short wavelength $\mathcal{O}(a)$ dominating (left). After “cooling” by 25 steps, 3 I ’s and 2 \bar{I} ’s may be clearly identified as bumps in the Lagrange density (middle) and the topological charge density (right).

Since the action is independent of the collective coordinates, one has to integrate over them and obtains the I -contribution $Z^{(I)}$, normalized to the topologically trivial perturbative contribution $Z^{(0)}$, in the form³

$$\frac{1}{Z^{(0)}} \frac{dZ^{(I)}}{d^4x} = \int_0^\infty d\rho D_m(\rho) \int dU. \quad (7)$$

The size distribution $D_m(\rho)$ is known in the framework of I -perturbation theory for small $\alpha_s(\mu_r) \ln(\rho \mu_r)$ and small $\rho m_i(\mu_r)$, where $m_i(\mu_r)$ are the running quark masses and μ_r denotes the renormalization scale. After its pioneering evaluation at 1-loop [2] for $N_c = 2$ and its generalization [14] to arbitrary N_c , it is meanwhile available [15] in 2-loop renormalization-group (RG) invariant form, i.e. $D^{-1} dD/d\ln(\mu_r) = \mathcal{O}(\alpha_s^2)$,

$$\frac{dn_I}{d^4x d\rho} = D_m(\rho) = D(\rho) \prod_{i=1}^{n_f} (\rho m_i(\mu_r)) (\rho \mu_r)^{n_f \gamma_0 \frac{\alpha_{\overline{\text{MS}}}(\mu_r)}{4\pi}}, \quad (8)$$

with the reduced size distribution

$$D(\rho) = \frac{d_{\overline{\text{MS}}}}{\rho^5} \left(\frac{2\pi}{\alpha_{\overline{\text{MS}}}(\mu_r)} \right)^{2N_c} \exp \left(-\frac{2\pi}{\alpha_{\overline{\text{MS}}}(\mu_r)} \right) (\rho \mu_r)^{\beta_0 + (\beta_1 - 4N_c \beta_0) \frac{\alpha_{\overline{\text{MS}}}(\mu_r)}{4\pi}}. \quad (9)$$

Here, γ_0 is the leading anomalous dimension coefficient, β_i ($i = 0, 1$) denote the leading and next-to-leading β -function coefficients and $d_{\overline{\text{MS}}}$ is a known [16] constant.

The powerlaw behaviour of the (reduced) I -size distribution,

$$D(\rho) \sim \rho^{\beta_0 - 5 + \mathcal{O}(\alpha_s)}, \quad (10)$$

generically causes the dominant contributions to the I -size integrals (e.g. Eq. (7)) to originate from the infrared (IR) regime (large ρ) and thus often spoils the applicability of I -perturbation

³For notational simplicity, we call the I -position in the following x (instead of x_0).

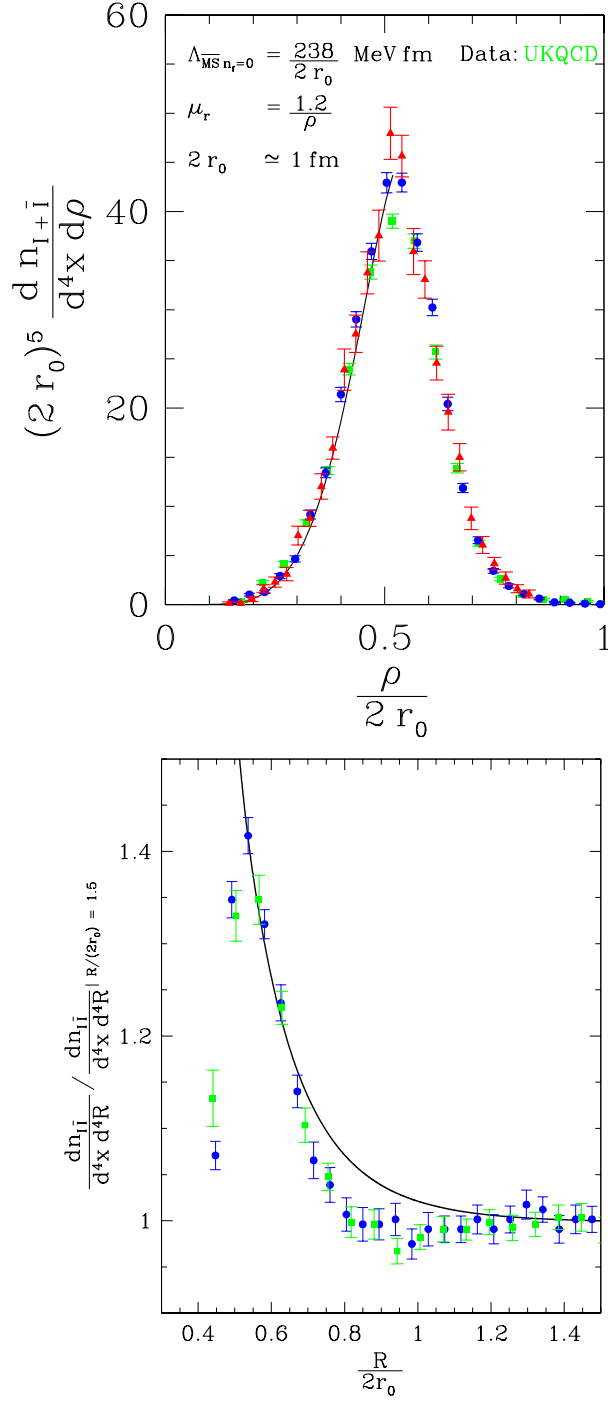


Figure 2: Continuum limit [11] of “equivalent” UKQCD data [12, 18] for the $(I + \bar{I})$ -size distribution (top) and the normalized $I\bar{I}$ -distance distribution (bottom) along with the respective predictions from I -perturbation theory and the valley form of the $I\bar{I}$ -interaction [11]. The 3-loop form of $\alpha_{\overline{\text{MS}}}$ with $\Lambda_{\overline{\text{MS}}}^{(0)}$ from ALPHA [19] was used.

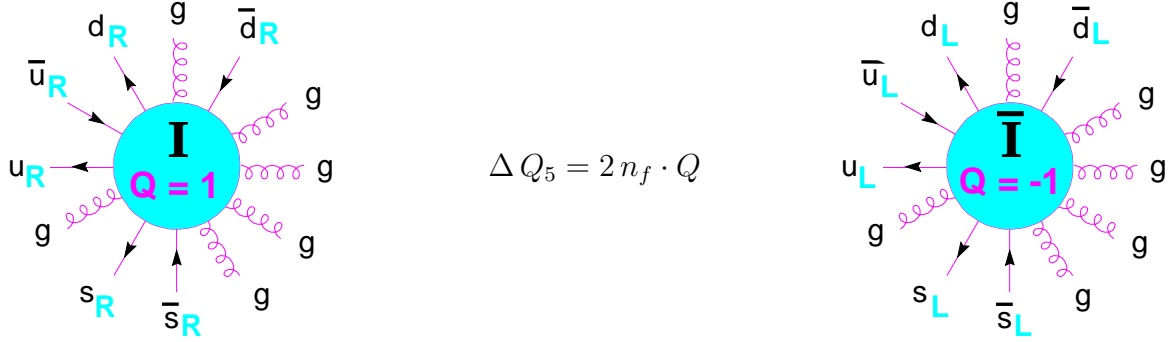


Figure 3: Instantons and anti-instantons induce chirality violating amplitudes.

theory. Since the I -size distribution not only appears in the vacuum-to-vacuum amplitude (7), but also in generic instanton-induced scattering amplitudes (c.f. Sect. 3) and matrix elements, it is extremely important to know the region of validity of the perturbative result (9).

Crucial information on the range of validity comes [11] from a recent high-quality lattice investigation [12] on the topological structure of the QCD vacuum (for $n_f = 0$). In order to make I -effects visible in lattice simulations with given lattice spacing a , the raw data have to be “cooled” first. This procedure is designed to filter out (dominating) fluctuations of short wavelength $\mathcal{O}(a)$, while affecting the topological fluctuations of much longer wavelength $\rho \gg a$ comparatively little. After cooling, an ensemble of I 's and \bar{I} 's can clearly be seen (and studied) as bumps in the Lagrange density and in the topological charge density (c.f. Fig. 1).

Figure 2 (top) illustrates the striking agreement in shape and normalization [11] of $2D(\rho)$ with the continuum limit of the UKQCD lattice data [12] for $dn_{I+\bar{I}}/d^4x d\rho$, for $\rho \lesssim 0.3 - 0.35$ fm. The predicted normalization of $D(\rho)$ is very sensitive to $\Lambda_{\overline{\text{MS}}}^{(0)}$ for which we took the most accurate (non-perturbative) result from ALPHA [19]. The theoretically favoured choice $\mu_r \rho = \mathcal{O}(1)$ in Fig. 2 (top) optimizes the range of agreement, extending right up to the peak around $\rho \simeq 0.5$ fm. However, due to its two-loop renormalization-group invariance, $D(\rho)$ is almost independent of μ_r for $\rho \lesssim 0.3$ fm over a wide μ_r range. Hence, for $\rho \lesssim 0.3$ fm, there is effectively no free parameter involved.

Turning back to the perturbative size distribution (8) in QCD with $n_f \neq 0$ light quark flavours, we would like to comment on the apparent suppression of the instanton-induced vacuum-to-vacuum amplitude (7) for small quark masses, $\rho m_i \ll 1$. It is related [2] to the axial anomaly [20] according to which any gauge field fluctuation with topological charge Q must be accompanied by a corresponding change in chirality,

$$\Delta Q_{5i} = 2Q; \quad i = 1, \dots, n_f. \quad (11)$$

Thus, pure vacuum-to-vacuum transitions induced by instantons are expected to be rare. On the other hand, scattering amplitudes or Green's functions corresponding to anomalous chirality violation (c.f. Fig. 3) are expected to receive their main contribution due to instantons and do not suffer from any mass suppression.

Let us illustrate this by the simplest example of one light flavour ($n_f = 1$): The instanton contribution to the fermionic two-point function can be written as

$$\langle \psi(x_1) \bar{\psi}(x_2) \rangle^{(I)} \simeq \int d^4x \int_0^\infty d\rho D(\rho) \int dU (\rho m) S^{(I)}(x_1, x_2; x, \rho, U). \quad (12)$$

Expressing the quark propagator in the I -background, $S^{(I)}$, in terms of the spectrum of the Dirac operator in the I -background, which has exactly one right-handed zero mode⁴ κ_0 [2],

$$-i \mathcal{D}^{(I)} \kappa_n = \lambda_n \kappa_n; \quad \text{with } \lambda_0 = 0 \text{ and } \lambda_n \neq 0 \text{ for } n \neq 0, \quad (13)$$

$$S^{(I)}(x_1, x_2; \dots) = \frac{\kappa_0(x_1; \dots) \kappa_0^\dagger(x_2; \dots)}{m} + \sum_{n \neq 0} \frac{\kappa_n(x_1; \dots) \kappa_n^\dagger(x_2; \dots)}{m + i\lambda_n}, \quad (14)$$

we see that for $m \rightarrow 0$ only the zero mode contribution survives in Eq. (12),

$$\langle \psi(x_1) \bar{\psi}(x_2) \rangle^{(I)} \simeq \int d^4x \int_0^\infty d\rho D(\rho) \int dU \rho \kappa_0(x_1; x, \rho, U) \kappa_0^\dagger(x_2; x, \rho, U). \quad (15)$$

Note that $\kappa_0 \kappa_0^\dagger$ has $Q_5 = 2$, exactly as required by the anomaly (11). For the realistic case of three light flavours ($n_f = 3$), the generalization of Eq. (15) leads to non-vanishing, chirality violating six-point functions corresponding to the anomalous processes shown in Fig. 3.

Finally, let us turn to the interaction between instantons and anti-instantons. In the instanton-anti-instanton ($I\bar{I}$) valley approach [22] it is determined in the following way: Starting from the infinitely separated ($R \rightarrow \infty$) $I\bar{I}$ -pair,

$$A_\mu^{(I\bar{I})}(x; \rho, \bar{\rho}, U, R) \stackrel{R \rightarrow \infty}{\simeq} A_\mu^{(I)}(x; \rho, \mathbf{1}) + A_\mu^{(\bar{I})}(x - R; \bar{\rho}, U) \quad (16)$$

one looks for a constraint solution, which is the minimum of the action for fixed collective coordinates, $\rho, \bar{\rho}, U, R$. The valley equations have meanwhile been solved for arbitrary separation R [23] and arbitrary relative color orientation U [24]. Due to classical conformal invariance, the $I\bar{I}$ -action $S^{(I\bar{I})}$ and the interaction Ω ,

$$S[A_\mu^{(I\bar{I})}] = \frac{4\pi}{\alpha_s} S^{(I\bar{I})}(\xi, U) = \frac{4\pi}{\alpha_s} (1 + \Omega(\xi, U)) \quad (17)$$

depend on the sizes and the separation only through the ‘‘conformal separation’’,

$$\xi = \frac{R^2}{\rho \bar{\rho}} + \frac{\bar{\rho}}{\rho} + \frac{\rho}{\bar{\rho}}. \quad (18)$$

Because of the smaller action, the most attractive relative orientation (c.f. Fig. 4) dominates in the weak coupling regime. Thus, in this regime, nothing prevents instantons and anti-instantons from approaching each other and annihilating.

⁴According to an index theorem [21], the number $n_{R/L}$ of right/left-handed zero modes of the Dirac operator in the background of a gauge field with topological charge Q satisfies $n_R - n_L = Q$. For the instanton: $n_R = Q = 1$; $n_L = 0$.

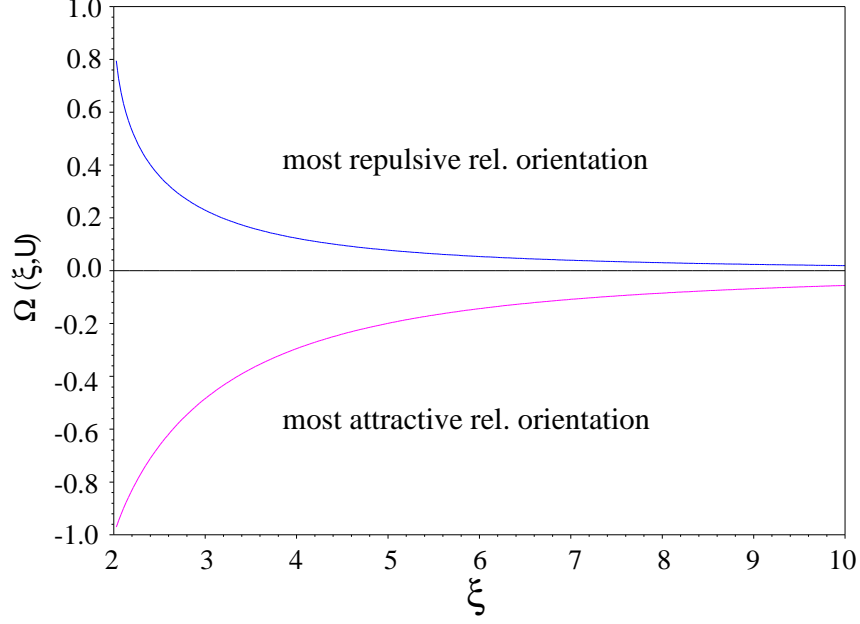


Figure 4: The instanton-anti-instanton interaction as a function of the conformal separation ξ , for the most attractive and the most repulsive relative orientation, respectively.

From a perturbative expansion of the path integral about the $I\bar{I}$ -valley, one obtains the contribution of the $I\bar{I}$ -valley to the partition function (2) in the form

$$\frac{1}{Z^{(0)}} \frac{dZ^{(I\bar{I})}}{d^4x} = \int d^4R \int_0^\infty d\rho \int_0^\infty d\bar{\rho} D_{I\bar{I}}(R, \rho, \bar{\rho}), \quad (19)$$

where the group-averaged distribution of $I\bar{I}$ -pairs, $D_{I\bar{I}}(R, \rho, \bar{\rho})$, is known, for small α_s , m_i , and for sufficiently large R [9, 10, 11],

$$\begin{aligned} \frac{dn_{I\bar{I}}}{d^4x d^4R d\rho d\bar{\rho}} &\simeq D_{I\bar{I}}(R, \rho, \bar{\rho}) = \\ &D(\rho) D(\bar{\rho}) \int dU \exp \left[-\frac{4\pi}{\alpha_{\overline{\text{MS}}}(s_{I\bar{I}}/\sqrt{\rho\bar{\rho}})} \Omega \left(\frac{R^2}{\rho\bar{\rho}}, \frac{\bar{\rho}}{\rho}, U \right) \right] \omega(\xi, U)^{2n_f}. \end{aligned} \quad (20)$$

Here, the scale factor $s_{I\bar{I}} = \mathcal{O}(1)$ parametrizes the residual scheme dependence and

$$\omega = \int d^4x \kappa_{0I}^\dagger(x; \dots) [\mathcal{D}^{(I\bar{I})}] \kappa_{0\bar{I}}(x - R; \dots) \quad (21)$$

denotes the fermionic interaction induced by the quark zero modes.

We will see below in Sect. 3 that the distribution (20) is a crucial input for instanton-induced scattering cross sections. Thus, it is extremely welcome that the range of validity of (20) can be inferred from a comparison with recent lattice data. Fig. 2 (bottom) displays the continuum limit [11] of the UKQCD data [12, 18] for the distance distribution of $I\bar{I}$ -pairs, $dn_{I\bar{I}}/d^4x d^4R$, along

with the theoretical prediction [11]. The latter involves (numerical) integrations of $\exp(-4\pi/\alpha_s \cdot \Omega)$ over the $I\bar{I}$ relative color orientation (U), as well as ρ and $\bar{\rho}$. For the respective weight $D(\rho)D(\bar{\rho})$, a Gaussian fit to the lattice data was used in order to avoid convergence problems at large $\rho, \bar{\rho}$. We note a good agreement with the lattice data down to $I\bar{I}$ -distances $R/\langle\rho\rangle \simeq 1$. These results imply first direct support for the validity of the “valley”-form of the interaction Ω between $I\bar{I}$ -pairs.

In summary: The striking agreement of the UKQCD lattice data with I -perturbation theory is a very interesting result by itself. The extracted lattice constraints on the range of validity of I -perturbation theory can be directly translated into a “fiducial” kinematical region for our predictions [9, 11] in deep-inelastic scattering, as shall be discussed in the next section.

3 Instantons in Deep-Inelastic Scattering

In this section we shall elucidate the special rôle of deep-inelastic scattering for instanton physics. We shall outline that only small size instantons, which are theoretically under contról, are probed in deep-inelastic scattering [8]. Furthermore, we shall show that suitable cuts in the Bjorken variables of instanton-induced scattering processes⁵ allow us to stay within the range of validity of instanton perturbation theory, as inferred from the lattice [9, 10]. We review the basic theoretical inputs to QCDINS, a Monte Carlo generator for instanton-induced processes in deep-inelastic scattering [5, 13]. Finally, we discuss the final state characteristics of instanton-induced events.

Let us consider a generic I -induced process in deep-inelastic scattering (DIS),

$$\gamma^* + g \Rightarrow \sum_{\text{flavours}}^{n_f} [\bar{q}_R + q_R] + n_g g, \quad (22)$$

which violates chirality according to the anomaly (11). The corresponding scattering amplitude is calculated as follows [8]: The respective Green’s function is first set up according to instanton perturbation theory in Euclidean position space, then Fourier transformed to momentum space, LSZ amputated, and finally continued to Minkowski space where the actual on-shell limits are taken. Again, the amplitude appears in the form of an integral over the collective coordinates [8],

$$\mathcal{T}_\mu^{(I)(2n_f+n_g)} = \int_0^\infty d\rho D(\rho) \int dU \mathcal{A}_\mu^{(I)(2n_f+n_g)}(\rho, U). \quad (23)$$

In leading order, the momentum dependence of the amplitude for fixed ρ and U ,

$$\mathcal{A}_\mu^{(I)(2n_f+n_g)}(q, p; k_1, k_2, \dots, k_{2n_f}, p_1, \dots, p_{n_g}; \rho, U), \quad (24)$$

factorizes, as illustrated in Fig. 5 for the case $n_f = 1$: The amplitude decomposes into a product of Fourier transforms of classical fields (instanton gauge fields; quark zero modes, e.g. as in Eq. (15))

⁵Our approach, focussing on the I -induced final state, differs substantially from an exploratory paper [25] on the I -contribution to the (inclusive) parton structure functions. Ref. [25] involves implicit integrations over the Bjorken variables of the I -induced scattering process. Unlike our approach, the calculations in Ref. [25] are therefore bound to break down in the interesting domain of smaller $x_{Bj} \lesssim 0.3$, where most of the data are located.

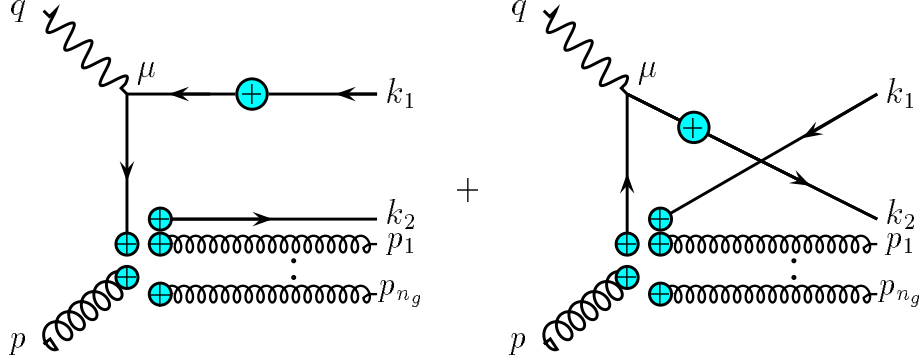


Figure 5: Instanton-induced chirality-violating process, $\gamma^*(q) + g(p) \rightarrow \bar{q}_R(k_1) + q_R(k_2) + g(p_1) + \dots + g(p_{n_g})$, for $n_f = 1$ in leading order of I -perturbation theory. The corresponding Green's function involves the products of the appropriate classical fields (lines ending at blobs) as well as the (non-zero mode) quark propagator in the instanton background (quark line with central blob).

and effective photon-quark “vertices” $\mathcal{V}_\mu^{(t(u))}(q, -k_{1(2)}; \rho, U)$, involving the (non-zero mode) quark propagator [26] in the instanton background. These vertices are most important in the following argumentation since they are the only place where the space-like virtuality $-q^2 = Q^2 > 0$ of the photon enters.

After a long and tedious calculation one finds [8] for these vertices,

$$\mathcal{V}_\mu^{(t)}(q, -k_1; \rho, U) = 2\pi i \rho^{3/2} [\epsilon \sigma_\mu \bar{V}(q, k_1; \rho) U^\dagger], \quad (25)$$

$$\mathcal{V}_\mu^{(u)}(q, -k_2; \rho, U) = 2\pi i \rho^{3/2} [UV(q, k_2; \rho) \bar{\sigma}_\mu \epsilon], \quad (26)$$

where

$$V(q, k; \rho) = \left[\frac{(q-k)}{-(q-k)^2} + \frac{k}{2q \cdot k} \right] \rho \sqrt{-(q-k)^2} K_1 \left(\rho \sqrt{-(q-k)^2} \right) - \frac{k}{2q \cdot k} \rho \sqrt{-q^2} K_1 \left(\rho \sqrt{-q^2} \right). \quad (27)$$

Here comes the crucial observation: Due to the (large) space-like virtualities $Q^2 = -q^2 > 0$ and $Q'^2 = -(q-k)^2 \geq 0$ in DIS and the exponential decrease of the Bessel K -function for large arguments in Eq. (27), the I -size integration in our perturbative expression (23) for the amplitude is effectively cut off. Only small size instantons, $\rho \sim 1/Q$, are probed in DIS and the predictivity of I -perturbation theory is retained for sufficiently large $\mathcal{Q} = \min(Q, Q')$.

The leading⁶ instanton-induced process in the DIS regime of $e^\pm P$ scattering for large photon virtuality Q^2 is illustrated in Fig. 6. The inclusive I -induced cross section can be expressed as

⁶ I -induced processes initiated by a quark from the proton are suppressed by a factor of α_s^2 with respect to the gluon initiated process [9]. This fact, together with the high gluon density in the relevant kinematical domain at HERA, justifies to neglect quark initiated processes.

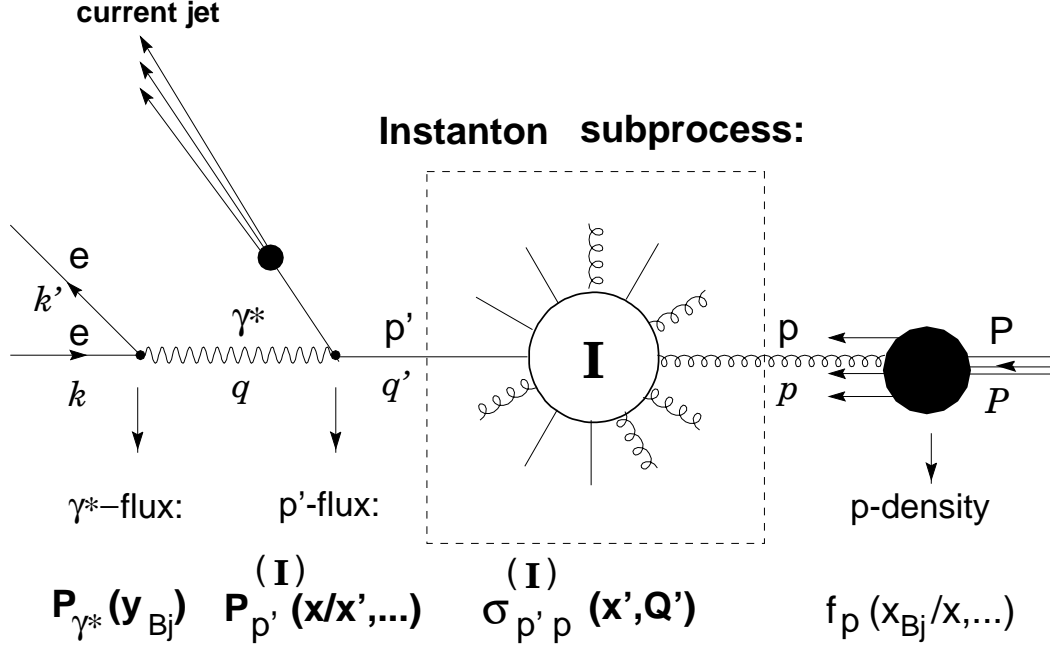


Figure 6: The leading instanton-induced process in the deep-inelastic regime of $e^\pm P$ scattering ($n_f = 3$).

a convolution [4, 9], involving integrations over the target-gluon density, f_g , the virtual photon flux, P_{γ^*} , and the known [9, 10] flux $P_{q'}^{(I)}$ of the virtual quark q' in the I -background (c.f. Fig. 6). The crucial instanton-dynamics resides in the so-called instanton-subprocess (c.f. dashed box in Fig. 6) with its associated total cross section $\sigma_{q'g}^{(I)}(Q', x')$, depending on its own Bjorken variables,

$$Q'^2 = -q'^2 \geq 0; \quad x' = \frac{Q'^2}{2p \cdot q'} \leq 1. \quad (28)$$

The cross section is obtained [9, 10] in the form of an integral over $I\bar{I}$ collective coordinates⁷,

$$\begin{aligned} \sigma_{q'g}^{(I)} \sim & \int d^4R \int_0^\infty d\rho \int_0^\infty d\bar{\rho} D(\rho) D(\bar{\rho}) \int dU e^{-\frac{4\pi}{\alpha_s} \Omega\left(\frac{R^2}{\rho\bar{\rho}}, \frac{\bar{\rho}}{\rho}, U\right)} \omega\left(\frac{R^2}{\rho\bar{\rho}}, \frac{\bar{\rho}}{\rho}, U\right)^{2n_f-1} \\ & \times e^{-Q'(\rho+\bar{\rho})} e^{i(p+q') \cdot R} \{ \dots \}. \end{aligned} \quad (29)$$

Thus, as anticipated in Sect. 2, the group averaged distribution of $I\bar{I}$ -pairs (20) is closely related to the instanton-induced cross section. The lattice constraints on this quantity are therefore extremely useful.

⁷Both an instanton and an anti-instanton enter here, since cross sections result from taking the modulus squared of an amplitude in the single I -background. In the present context, the $I\bar{I}$ -interaction Ω takes into account the exponentiation of final state gluons [9].

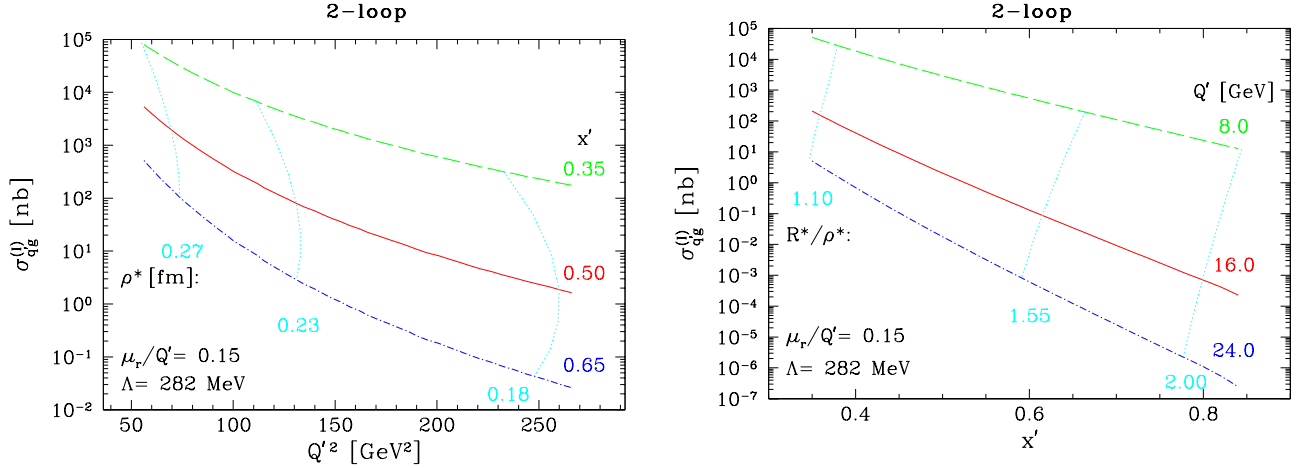


Figure 7: I -subprocess cross section [9] displayed versus the Bjorken variable Q'^2 with x' fixed (left) and versus x' with Q'^2 fixed (right) for $n_f = 3$. The dotted lines indicate the corresponding effective I -sizes ρ^* [fm] (left) and $I\bar{I}$ -distances R^* in units of ρ^* (right), respectively.

Again, the quark virtuality Q'^2 cuts off large instantons. Hence, the integrals in (29) are finite. In fact, they are dominated by a unique saddle-point [9, 10],

$$\begin{aligned}
 U^* &= \text{most attractive relative orientation;} \\
 \rho^* &= \bar{\rho}^* \sim 1/Q'; \quad R^{*2} \sim 1/(p+q')^2 \Rightarrow \frac{R^*}{\rho^*} \sim \sqrt{\frac{x'}{1-x'}}, \quad (30)
 \end{aligned}$$

from which it becomes apparent (c.f. Fig. 7) that the virtuality Q' controls the effective I -size, while x' determines the effective $I\bar{I}$ -distance (in units of the size ρ). By means of the discussed saddle-point correspondence (30), the lattice constraints may be converted into a “fiducial” region for our cross section predictions in DIS [9],

$$\left. \begin{aligned} \rho^* &\lesssim 0.3 - 0.35 \text{ fm;} \\ \frac{R^*}{\rho^*} &\gtrsim 1 \end{aligned} \right\} \Rightarrow \left\{ \begin{aligned} Q'/\Lambda_{\overline{\text{MS}}}^{(n_f)} &\gtrsim 30.8; \\ x' &\gtrsim 0.35. \end{aligned} \right. \quad (31)$$

As illustrated in Fig. 7, $\sigma_{q'g}^{(I)}(Q', x')$ is very steeply growing for decreasing values of Q'^2 and x' , respectively. The constraints (31) from lattice simulations are extremely valuable for making concrete predictions. Note that the fiducial region (31) and thus all our predictions for HERA never involve values of the $I\bar{I}$ -interaction Ω smaller than -0.5 (c.f. Fig. 4), a value often advocated as a lower reliability bound [27].

Let us present an update of our published prediction [9] of the I -induced cross section at HERA. For the following *modified* standard cuts,

$$\begin{aligned}
 \mathcal{C}_{\text{std}} &= x' \geq 0.35, \quad Q' \geq 30.8 \Lambda_{\overline{\text{MS}}}^{(n_f)}, \quad x_{\text{Bj}} \geq 10^{-3}, \\
 &0.1 \leq y_{\text{Bj}} \leq 0.9, \quad Q \geq 30.8 \Lambda_{\overline{\text{MS}}}^{(n_f)}, \quad (32)
 \end{aligned}$$

involving the minimal cuts (31) extracted from lattice simulations, and an update of $\Lambda_{\overline{\text{MS}}}$ to the 1998 world average [28], we obtain

$$\sigma_{\text{HERA}}^{(I)}(\mathcal{C}_{\text{std}}) = 29.2_{-8.1}^{+9.9} \text{ pb.} \quad (33)$$

Note that the quoted errors in the cross section (33) only reflect the uncertainty in $\Lambda_{\overline{\text{MS}}}^{(5)} = 219_{-23}^{+25}$ MeV [28], on which $\sigma^{(I)}$ is known to depend very strongly [9]. We have also used now the 3-loop formalism [28] to perform the flavour reduction of $\Lambda_{\overline{\text{MS}}}^{(n_f)}$ from 5 to 3 light flavours. Finally, the value of $\sigma^{(I)}$ is substantially reduced compared to the one in Ref. [9], since we preferred to introduce a further cut in Q^2 , with $Q_{\text{min}}^2 = Q_{\text{min}}^{\prime 2}$, in order to insure the smallness of the I -size ρ in contributions associated with the second term in Eq. (27).

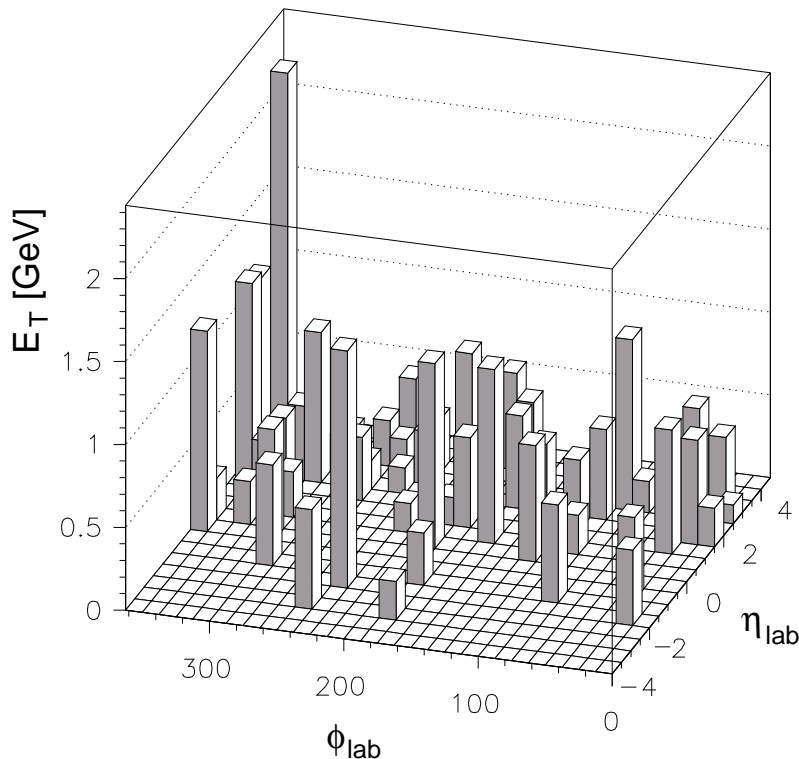


Figure 8: Lego plot of a typical instanton-induced event from QCDINS.

Based on the predictions of I -perturbation theory, a Monte Carlo generator for simulating QCD-instanton induced scattering processes in DIS, QCDINS, has been developed [5, 13]. It is designed as an “add-on” hard process generator interfaced by default to the Monte Carlo generator HERWIG [29]. Optionally, an interface to JETSET [30] is also available for the final hadronization step.

QCDINS incorporates the essential characteristics that have been derived theoretically for the hadronic final state of I -induced processes: notably, the isotropic production of the partonic final

state in the I -rest system ($q'g$ center of mass system in Fig. 6), flavour “democracy”, energy weight factors different for gluons and quarks, and a high average multiplicity $2n_f + \mathcal{O}(1/\alpha_s)$ of produced partons with a (approximate) Poisson distribution of the gluon multiplicity.

The characteristic features of the I -induced final state are illustrated in Fig. 8 displaying the lego plot of a typical event from QCDINS (c.f. also Fig. 6): Besides a single (not very hard) current jet, one expects an accompanying densely populated “hadronic band”. For $x_{\text{Bj min}} \simeq 10^{-3}$, say, it is centered around $\bar{\eta} \simeq 2$ and has a width of $\Delta\eta \simeq \pm 1$. The band directly reflects the isotropic production of an I -induced “fireball” of $\mathcal{O}(10)$ partons in the I -rest system. Both the total transverse energy $\langle E_T \rangle \simeq 15$ GeV and the charged particle multiplicity $\langle n_c \rangle \simeq 13$ in the band are far higher than in normal DIS events. Finally, each I -induced event has to contain strangeness such that the number of K^0 's amounts to $\simeq 2.2/\text{event}$.

4 Search Strategies

In a recent detailed study [7], based on QCDINS and standard DIS event generators, a number of basic (experimental) questions have been investigated: How to isolate an I -enriched data sample by means of cuts to a set of observables? How large are the dependencies on Monte-Carlo models, both for I -induced (INS) and normal DIS events? Can the Bjorken-variables (Q' , x') of the I -subprocess be reconstructed?

All the studies presented in Ref. [7] were performed in the hadronic center of mass frame, which is a suitable frame of reference in view of a good distinction between I -induced and normal DIS events (c.f. Ref. [6]). The results are based on a study of the hadronic final state, with typical acceptance cuts of a HERA detector being applied.

Let us briefly summarize the main results of Ref. [7]. While the “ I -separation power” = $\text{INS}_{\text{eff(iciency)}}/\text{DIS}_{\text{eff(iciency)}}$ typically does not exceed $\mathcal{O}(20)$ for single observable cuts, a set of six observables (among ~ 30 investigated in Ref. [6]) with much improved joint I -separation power = $\mathcal{O}(130)$ could be found, see Fig. 9. These are (a) the p_T of the current jet, (b) Q'^2 as reconstructed from the final state, (c) the transverse energy and (d) the number of charged particles in the I -band region⁸, and (e,f) two shape observables that are sensitive to the event isotropy.

The systematics induced by varying the modelling of I -induced events remains surprisingly small (Fig. 10). In contrast, the modelling of normal DIS events in the relevant region of phase space turns out to depend quite strongly on the used generators and parameters [7]. Despite a relatively high expected rate for I -events in the fiducial DIS region [9], a better understanding of the tails of distributions for normal DIS events turns out to be quite important.

⁸With the prime in Fig. 9 (c,d,e) indicating that the hadrons from the current jet have been subtracted.

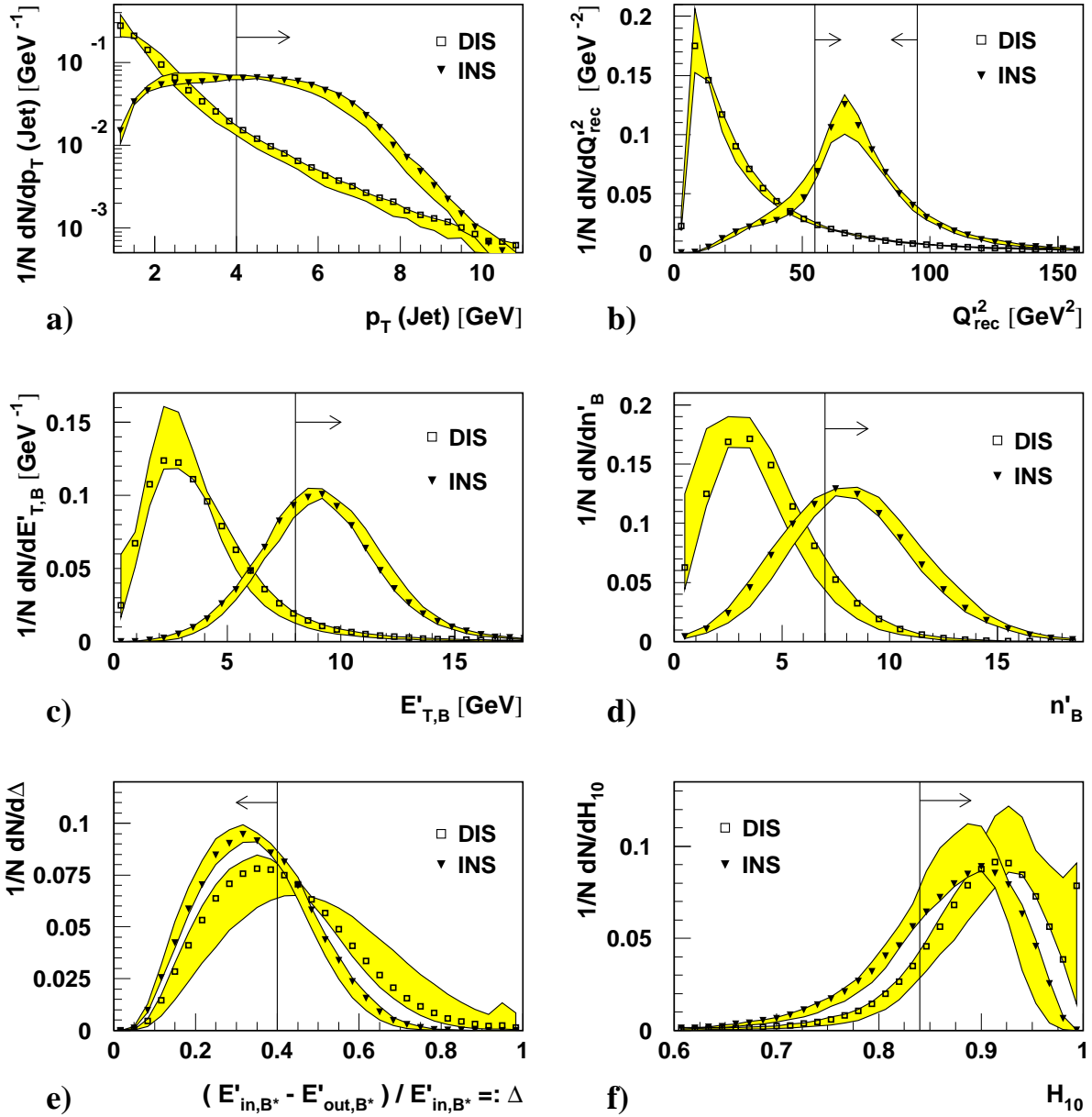


Figure 9: Distributions of various observables for normal DIS and I -induced processes [7]. Shown are the distributions for the “reference Monte Carlos” (INS markers = QCDINS + HERWIG, DIS markers = ARIADNE [31], including Pomeron exchange) and their variations (shaded band) resulting from the choice of different models or the variation of parameters of a model (c.f. Fig. 10). The lines and the corresponding arrows show the cut applied in each of the observables, with the arrows pointing in the direction of the allowed region.

Cuts:

$$55 \text{ GeV}^2 < Q_{\text{rec}}^2 < 95 \text{ GeV}^2$$

$$p_T(\text{Jet}) > 4 \text{ GeV}$$

$$E'_{T,B} > 8 \text{ GeV}$$

$$(E'_{\text{in},B^*} - E'_{\text{out},B^*}) / E'_{\text{in},B^*} < 0.4$$

$$H_{10} > 0.84$$

$$n'_B \geq 7$$

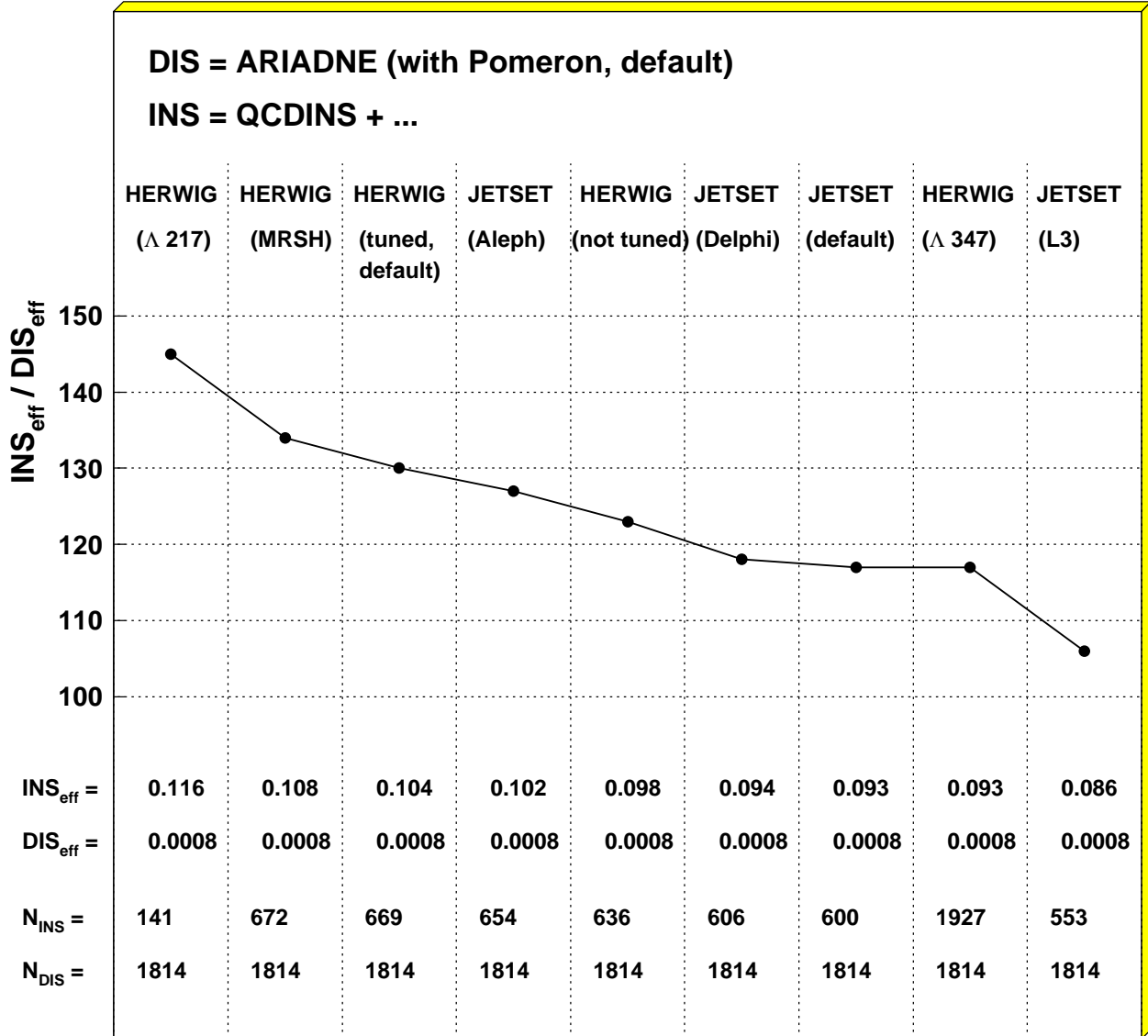


Figure 10: I -separation power ($INS_{\text{eff}}/DIS_{\text{eff}}$) of a multidimensional cut-scenario depending on the variation of MC models and parameters used to simulate I -induced events [7]. The efficiencies and remaining event numbers for an integrated luminosity $\mathcal{L} \simeq 30 \text{ pb}^{-1}$ and corresponding to the cross section from QCDINS 1.6.0 are listed.

References

- [1] A. Belavin, A. Polyakov, A. Schwarz, Yu. Tyupkin: Phys. Lett. B **59**, 85 (1975)
- [2] G. 't Hooft: Phys. Rev. Lett. **37**, 8 (1976); Phys. Rev. D **14**, 3432 (1976); Phys. Rev. D **18**, 2199 (1978) (Erratum); Phys. Rep. **142**, 357 (1986)
- [3] T. Schäfer, E. Shuryak: Rev. Mod. Phys. **70**, 323 (1998)
- [4] A. Ringwald, F. Schrempp: 'Towards the Phenomenology of QCD-Instanton Induced Particle Production at HERA', hep-ph/9411217. In: *Quarks '94, Proc. 8th Int. Seminar, Vladimir, Russia, May 11-18, 1994*, ed. by D. Grigoriev et al. (World Scientific, Singapore 1995) pp. 170-193
- [5] M. Gibbs, A. Ringwald, F. Schrempp: 'QCD-Instanton Induced Final States in Deep Inelastic Scattering', hep-ph/9506392. In: *Workshop on Deep Inelastic Scattering and QCD (DIS 95), Paris, France, April 24-28, 1995*, ed. by J.F. Laporte, Y. Sirois (Ecole Polytechnique, Paris 1995) pp. 341-344
- [6] J. Gerigk: 'QCD-Instanton-induzierte Prozesse in tiefunelastischer $e^\pm p$ -Streuung', Dipl. Thesis (in German), University of Hamburg (unpublished) and MPI-PhE/98-20, Nov. 1998
- [7] T. Carli, J. Gerigk, A. Ringwald, F. Schrempp: 'QCD Instanton-Induced Processes in Deep-Inelastic Scattering – Search Strategies and Model Dependencies', hep-ph/9906441. To appear in: *Proc. DESY Workshop 1998/1999 on Monte Carlo Generators for HERA Physics*
- [8] S. Moch, A. Ringwald, F. Schrempp: Nucl. Phys. B **507**, 134 (1997)
- [9] A. Ringwald, F. Schrempp: Phys. Lett. B **438**, 217 (1998)
- [10] S. Moch, A. Ringwald, F. Schrempp: in preparation
- [11] A. Ringwald, F. Schrempp: Phys. Lett. B **459**, 249 (1999)
- [12] D.A. Smith, M.J. Teper (UKQCD): Phys. Rev. D **58**, 014505 (1998)
- [13] A. Ringwald, F. Schrempp: in preparation
- [14] C. Bernard: Phys. Rev. D **19**, 3013 (1979)
- [15] T. Morris, D. Ross, C. Sachrajda: Nucl. Phys. B **255**, 115 (1985)
- [16] A. Hasenfratz, P. Hasenfratz: Nucl. Phys. B **193**, 210 (1981)
M. Lüscher: Nucl. Phys. B **205**, 483 (1982)
- [17] M.-C. Chu, J.M. Grandy, S. Huang, J.W. Negele: Phys. Rev. D **49**, 6039 (1994)
- [18] M. Teper: private communication

- [19] S. Capitani, M. Lüscher, R. Sommer, H. Wittig: Nucl. Phys. B **544**, 669 (1999)
- [20] S. Adler: Phys. Rev. **177**, 2426 (1969)
J. Bell, R. Jackiw: Nuovo Cimento **51**, 47 (1969)
W. Bardeen: Phys. Rev. **184**, 1848 (1969)
- [21] M. Atiyah, I. Singer: Ann. Math. **87**, 484 (1968)
- [22] A. Yung: Nucl. Phys. B **297**, 47 (1988)
- [23] V.V. Khoze, A. Ringwald: Phys. Lett. B **259**, 106 (1991)
- [24] J. Verbaarschot: Nucl. Phys. B **362**, 33 (1991)
- [25] I. Balitsky, V. Braun: Phys. Lett. B **314**, 237 (1993)
- [26] L. Brown, R. Carlitz, D. Creamer, C. Lee: Phys. Rev. D **17**, 1583 (1978)
- [27] V. Zakharov: Nucl. Phys. B **353**, 683 (1991)
M. Maggiore, M. Shifman: Nucl. Phys. B **365**, 161 (1991); *ibid.* **371**, 177 (1991)
G. Veneziano: Mod. Phys. Lett. A **7**, 1661 (1992)
- [28] C. Caso et al. (Particle Data Group): Eur. Phys. J. C **3**, 1 (1998)
- [29] G. Marchesini et al.: Comp. Phys. Commun. **67**, 465 (1992)
- [30] T. Sjöstrand: Comp. Phys. Commun. **82**, 74 (1994)
- [31] L. Lönnblad: Comp. Phys. Commun. **71**, 15 (1992)